Catalysis Today 157 (2010) 191–197

Contents lists available at ScienceDirect

Catalysis Today

journal homepage: www.elsevier.com/locate/cattod

Use and observation of the hydrotalcite "memory effect" for VOC oxidation

C. Gennequin[a,b], T. Barakat[a,b], H.L. Tidahy[a,b], R. Cousin[a,b], J.-F. Lamonier[a,1], A. Aboukaïs[a,b], S. Siffert[a,b,*]

[a] Univ Lille Nord de France, F-59000 Lille, France
[b] ULCO, UCEIV, E.A. 4492, F-59140 Dunkerque, France

ARTICLE INFO

Article history:
Available online 14 April 2010

Keywords:
VOC
Oxidation
LDH
Cobalt
Hydrotalcite

ABSTRACT

Cobalt supported on calcined hydrotalcite catalysts were prepared using the memory effect of Mg–Al hydrotalcite. Mg–Al was calcined at different temperatures from 500 to 900 °C and dipped in a Co nitrate aqueous solution for surface hydrotalcite regeneration. The calcination at 500 °C of the sample Co/Mg–Al(700) leads to an interesting Co mixed oxide supported on calcined hydrotalcite with high specific area and highly active and selective for toluene oxidation. The surface Co hydrotalcite regeneration was observed especially by Infrared Spectroscopy and Scanning Electron Microscopy combined with Energy Dispersive detection of emitted X-ray photons. The reconstruction of the layered structure influences positively the iteraction between cobalt species and the support.

1. Introduction

VOC (Volatile Organic Compounds) are recognized as major contributors to air pollution mostly not only because of their malodorous, toxic and carcinogenic nature but also because of their tendency to induce ozone formation. Environmental legislations are imposing increasingly stringent emission levels in order to limit VOC emissions into the atmosphere. The best three abatement technologies judged as efficient in controlling VOC emissions are absorption, catalytic oxidation and thermal incineration. Thermal incineration is left aside as it requires temperatures higher than 1100 °C and produces toxic fumes such as dioxins and nitrogen oxides. Alternatively, heterogeneous catalytic oxidation is considered to be a promising technique for VOC elimination [1,2], since the reaction is operated at much lower temperatures (200–450 °C) than those required for thermal incineration. Two types of catalysts are used in this technique: noble metal based systems [3–6] and metal oxide based systems [7–9]. Supported noble metal systems present a high activity for the oxidation of a large variety of VOCs, with a high selectivity for carbon oxides [10,11]. Nevertheless, the main challenges in the use of these systems reside in their high cost and their deactivation in the presence of chlorinated compounds in the waste stream [12]. Manganese and cobalt oxides are considered to be the most active transition metal oxides for VOC catalytic oxidation, although they are characterized by a low specific surface area and a poor thermal stability [8,9,11,13,14]. Supported cobalt catalysts are conventionally studied for hydrocarbon oxidation [15,16].

Furthermore, supports are also known for their important role in the improvement of catalytic activities, especially in oxidation reactions. Thus, hydrotalcite precursors provide a convenient means of obtaining supports with high specific areas, leading to well dispersed active phases and catalysts with interesting basic properties [17–20]. The structure of hydrotalcites can be derived from a brucite structure ($Mg(OH)_2$) [21] in which a part of the Mg^{2+} cations are substituted by a trivalent metal such as Al^{3+}. Partial or total substitution of Mg^{2+} and Al^{3+} can be carried out by divalent cations ($M^{2+} = Zn^{2+}$, Ni^{2+}, Cu^{2+}, Co^{2+}, ...) and trivalent cations ($M^{3+} = Fe^{3+}$, Cr^{3+}, ...), respectively. The positive charge of the metal hydroxide layers is compensated by interstitial layers built of anions ($A^{m-} = CO_3^{2+}$, NO_3^-, ...) and water molecules. Indeed, it has been shown that the calcination of layered double hydroxides (LDHs) at specific temperatures (depending on the particular cations in the layers and anions in the interlayer) leads to the formation of mixed oxides. These oxides are characterized by their structural homogeneity, absence of chemical segregation and their basic sites useful for catalysis [22,23]. The presence of acidic or basic sites on solids can affect the adsorption of VOC, and acidity plays a strong role in the catalytic oxidation. The acid–base properties of catalysts surface depend on the ionic or covalent character of metal oxygen bonds. Calcined mixed oxides (MgAlO) type exhibits various basic functionalities at the surface: weakly basic OH^- groups, medium to medium strong sites connected to the oxygen of Mg^{2+}–O^{2-} pairs and strong basic sites related to isolated O^{2-} anions. The fraction of medium–strong and strong sites increases with the Mg/Al ratio and a high temperature of calcination [20]. LDHs' ability to regenerate after moderate heating, often called "memory effect", is thought to

* Corresponding author at: Unité de Chimie Environnementale et Interactions sur le Vivant, Université du Littoral - Côte d'Opale, 145 Avenue Schumann, 59140 Dunkerque, France. Tel.: +33 03 28 65 82 56; fax: +33 03 28 65 82 39.
E-mail address: siffert@univ-littoral.fr (S. Siffert).
[1] Present address: USTL, UCCS, UMR CNRS 8181, F-59650 Villeneuve d'Ascq, France.

0920-5861/$ – see front matter © 2010 Elsevier B.V. All rights reserved.
doi:10.1016/j.cattod.2010.03.012

be one of the most interesting and useful properties. The formed mixed oxides are often amorphous, with a high specific surface area and an ability to recover the layered structure by simple contact with a water solution. Moreover, the reconstruction step of decomposed hydrotalcites and the exchange of counter anions have an impact on the basicity of the sample [20].

In one of our recent papers [25], cobalt based catalysts were synthesized using the "memory effect". The noticed interesting catalytic behaviour towards VOC oxidation was explained by their representative structure. In the present paper, further investigations were conducted for this type of catalysts in order to observe the hydrotalcite "memory effect" directly related to VOC oxidation. Toluene was chosen as a probe molecule for VOC oxidation testing, because it is often found in industrial exhausts and presents high Photochemical Ozone Creation Potentials (POCP).

2. Experimental

The support Mg–Al (HT) was prepared with an Mg/Al atomic ratio of 3/1 with adequate aqueous solution of the precursor salts. A sodium carbonate solution was then added, and the pH of the solution was adjusted at 10 by adding an aqueous solution of sodium hydroxide. The resulting slurry was heated at 60 °C for 24 h. Then, the precipitate was filtered, washed several times with hot deionized water (50 °C) and dried at 60 °C for 48 h. The dried precipitate was calcined at various temperatures. These supports were denoted Mg–Al(*T*) with *T* (calcination temperature) = 500, 600, 700, 800 and 900 °C.

5 wt% of metallic Co was then deposited on each support by aqueous impregnating method using cobalt nitrate. The impregnated powders are dried over night at 100 °C and calcined under airflow at 500 °C. The final products were called Co/Mg–Al(*T*)500.

Supports and catalysts were then characterized by several techniques: nitrogen adsorption–desorption, powder XRD, IR, SEM–EDX, H_2-TPR. VOCs oxidation was then performed with cobalt containing catalysts (100 mg per sample) from ambient temperature to 500 °C (1 °C min^{-1}) at atmospheric pressure. Before each test, the catalyst was reactivated in flowing air (2 L h^{-1}) at 500 °C for 4 h. The flow of the reactant gases (100 mL min^{-1} with 1000 ppm of C_7H_8 and balance with air) was adjusted by a Calibrage CALPC-5 apparatus constituted of a saturator and mass flow controllers. After reaching a stable flow, reactants passed through the catalyst bed and the temperature was increased from room temperature to 500 °C (1 °C min^{-1}). The feed and the reactor outflow gases were analyzed on line by a micro-gas chromatograph (VARIAN CP4900).

BET surface areas of the solids were measured by nitrogen adsorption at −196 °C using thermo-Electron Q surf M1 apparatus. The samples were outgassed for 2 h at 300 °C.

The structure of solids was analyzed at room temperature by X-ray diffraction (XRD) technique in a Brüker D8 Advance diffractometer equipped with a copper anode (λ = 1.5406 Å). The scattering intensities were measured over an angular range of $4° < 2\theta < 80°$ for all the samples with a step-size of $\Delta(2\theta) = 0.02°$ and a count time of 6 s per step. The diffraction patterns were indexed by comparison with the JCPDS files.

H_2-Temperature-Programmed Reduction (TPR) of the calcined catalysts was carried out in an Altamira AMI 200 apparatus. Prior to the TPR experiments, samples (30 mg) were activated under argon at 150 °C for 1 h. The samples were then heated from ambient to 900 °C under H_2 flow (5 vol.% in argon—30 mL min^{-1}) at a heating rate of 5 °C min^{-1}.

Scanning Electron Microscopy analysis was performed on a 438 VP microscope (LEO Cambridge) equipped with an Energy Dispersive X-ray spectrometer (SEM EDX IXRF). Typical working parameters were an accelerating voltage of 25 kV, and a beam current of 150 pA.

Fourier transform infrared absorption spectra were recorded using the KBr pellet technique on a FTIR Equinox 55 Brüker spectrometer in the range 4000–400 cm^{-1} and a resolution of 4 cm^{-1}.

3. Results and discussions

Previous results using XRD analysis of supports Mg–Al(500, 600 and 700) (Fig. 1) showed that hydrotalcite like structure is not detected for all samples (2θ = 11.27; 34.46°, JCPDS 220700) but XRD patterns revealed the formation of mixed oxides which are Mg(Al^{3+})O solid solutions of MgO–periclase type in agreement with JCPDS file no. 450946 [26]. In the case of samples calcined at higher temperature (800 and 900 °C), very weak diffraction lines corresponding to $MgAl_2O_4$ spinel structure (JCPDS no. 211152) are detected [27].

For dried Mg–Al hydrotalcite, the surface area is sharply increased from 77 to a value higher than 100 m^2/g after calcination (Table 1). The sample calcined at 500 °C (Mg–Al(500)) presents the highest surface area (214 m^2/g), and it is clear that S_{BET} value decreases gradually with increasing calcination temperature.

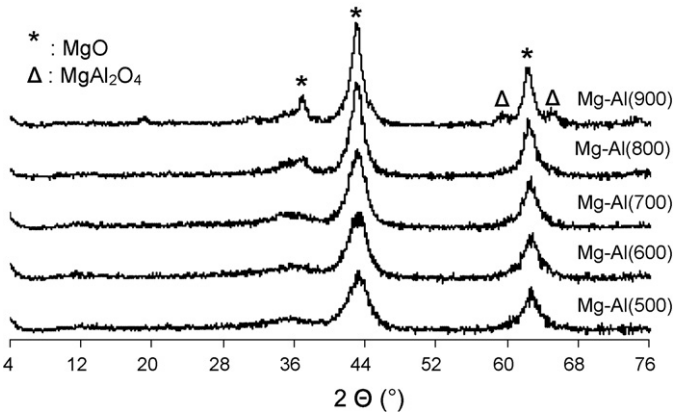

Fig. 1. XRD patterns of Mg–Al hydrotalcite calcined at 500–900 °C. Some patterns were already published in Ref. [24].

Table 1
Specific surface area of the samples, $d_{(003)}$ parameter and corresponding 2θ angle of the solids.

Samples	2θ (°)	$d_{(003)}$ (Å)	Specific area (m^2/g)
Mg–Al(HT)	11.38	7.76	77
Mg–Al(500)	–	–	214
Mg–Al(600)	–	–	188
Mg–Al(700)	–	–	132
Mg–Al(800)	–	–	122
Mg–Al(900)	–	–	112
Co/Mg–Al(500)	11.20	7.89	3
Co/Mg–Al(600)	11.58	7.63	4
Co/Mg–Al(700)	11.54	7.66	6
Co/Mg–Al(800)	10.24	8.63	82
Co/Mg–Al(900)	10.23	8.63	89
HT with Mg/Al = 2[a]	–	7.552	–
HT with Mg/Al = 2.5[a]	–	7.626	–
HT with Mg/Al = 3[a]	–	7.778	–
HT with Mg/Al = 3.5[a]	–	7.835	–
Co/Mg–Al(500)500	–	–	233
Co/Mg–Al(600)500	–	–	219
Co/Mg–Al(700)500	–	–	190
Co/Mg–Al(800)500	–	–	187
Co/Mg–Al(900)500	–	–	165

[a] Ref. [37].

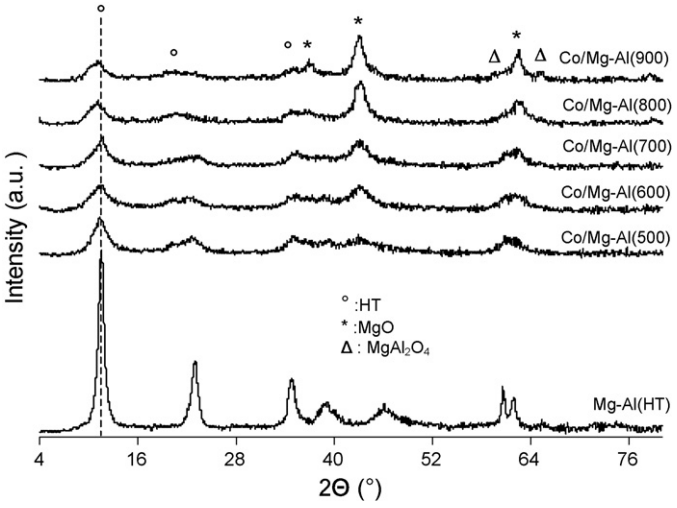

Fig. 2. XRD patterns of Mg–Al(HT) and Co/Mg–Al(*T*) (*T* = 500, 600, 700, 800 and 900 °C) dried samples. Some patterns were already published in Ref. [24].

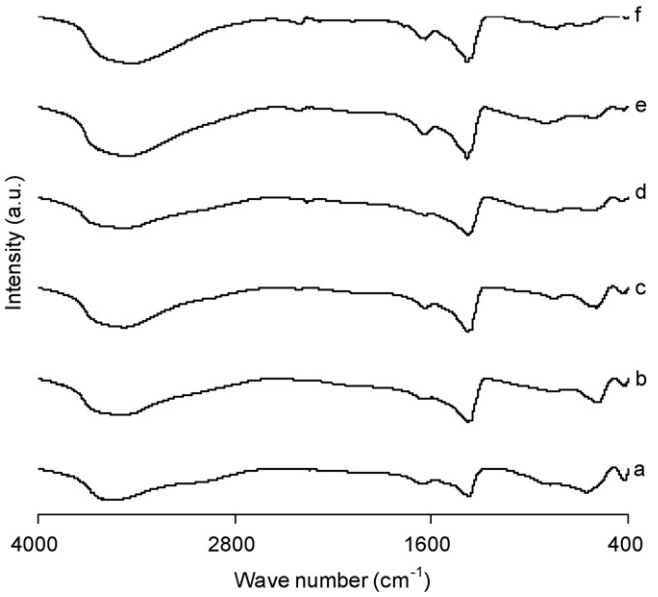

Fig. 3. IR spectra of Mg–Al(HT) and Co/Mg–Al(*T*) (*T* = 500, 600, 700, 800 and 900 °C). (a) Mg–Al(HT); (b) Co/Mg–Al(500); (c) Co/Mg–Al(600); (d) Co/Mg–Al(700); (e)Co/Mg–Al(800) and (f) Co/Mg–Al(900).

This result can be related to the higher crystallization of sample treated at higher temperature. Many authors [27–29] have already discussed this variation of specific area after thermal treatment of hydrotalcite. In fact, Yang et al. [29] supposed a thermal evolution of hydrotalcite-type Mg–Al (ratio Mg/Al = 2) leading to an amorphous phase around 400–600 °C and a solid solution of MgO type + Al_2O_3. And Staminirova et al. [27] suggested a thermal evolution of Mg–Al hydrotalcite (Mg/Al = 3) leading to a "metahydrotalcite P periclase amorphous" phase between 400 and 900 °C and a solid solution of MgO + $MgAl_2O_4$. In our case, "metahydrotalcite P periclase", which is an amorphous phase, may be present in each sample after any calcination temperature. Thus, this amorphous phase can be partly responsible for the high specific surface of our oxides. However, after calcination at 800 °C and 900 °C, the decrease of specific surface area is related to particles sintering and the emergence of mixed oxides with spinel structure ($MgAl_2O_4$, JCPDS no. 211152).

XRD patterns of dried Co/Mg–Al(*T*) (Fig. 2) reveal three distinct crystalline phases: MgO (JCPDS 450946), hydrotalcite phase (JCPDS 220700) and cobalt oxyhydroxide (JCPDS 731213). MgO structure is detected in all samples. Its presence is due to Mg–Al hydrotalcite calcination. However, this phase is weakly shifted towards high value of 2θ due to aluminium ions insertion in the lattice of MgO. The presence of hydrotalcite phase is related to the regeneration capacity of hydrotalcite induced by the presence of water, CO_2 and nitrates (dissolved in aqueous solution) during cobalt impregnation. This regeneration in aqueous solution, called also "the memory effect" of the hydrotalcite, was already described by our group [25].

Ion exchange between the cation in the regenerating solution and Mg^{2+} is also possible as suggested by Staminirova et al. [30]. Then after the reconstruction step, the chemical composition of octahedral layers of cobalt containing hydrotalcite is changed. This result is evidenced by the change of the "*a*" parameter value. In our case, this change is not obvious because solid reconstructions are only partial and XRD peak at $2\theta = 60°$ giving the average distance cation–cation in the layer of brucite type is overlapped with a peak attributed to MgO phase. Nevertheless, XRD results can also give information about the layer thickness. Thus, the first peak shows a shoulder and a dissymmetry at a value of 2θ around 11.4° probably due to the thick layer's heterogeneity of the regenerated hydrotalcite. During reconstruction process, anions like NO_3^- (from cobalt salt) and OH^- (from water) can be exchanged quantitatively with carbonate ions, and then a mixed anionic interstitial layer is created. The anionic composition is related to the composition of the regenerating solution and has a strong influence on the layer's thickness, which becomes larger. Consequently, the shoulder at 11.4° can be related to the rearrangement of anions in different symmetries in the interlayer thickness. And reconstructed sample shows a shift of 2θ value compared to the XRD pattern of the parent hydrotalcite (Fig. 2), due to the change of the ratio M^{2+}/M^{3+} after reconstruction.

Table 1 summarizes 2θ and lattice parameters "*d*", corresponding to (0 0 3) plane, of samples with Mg/Al ratio between 2 and 3.5. The value of parameter "*d*" increases with Mg/Al ratio, so 2θ is shifted to lower values. Thus, the reconstruction hypothesis of samples with a ratio M^{2+}/M^{3+} value different to 3 is quite probable because, in our case only partial reconstruction occurs whereas as part of the sample remains under the form of Mg(Al)O oxide. For Co/Mg–Al(800) and Co/Mg–Al(900) samples, 2θ shifts are more pronounced than those of samples calcined at lower temperatures; it is then possible that each reconstructed hydrotalcite has its own structure. Finally, regenerated structures possess Mg/Al ratio higher than 3 due to the presence of stable phase $MgAl_2O_4$, which does not participate to the reconstruction, only Mg(Al)O oxide type is concerned.

For a better understanding of the heterogeneity of the layer thickness of regenerated hydrotalcite, Infrared Spectroscopy was carried out. Fig. 3 shows IR spectra of Co/Mg–Al(*T*) catalysts, and for comparison purpose, Mg–Al (HT) spectrum is also shown. For the impregnated samples, the FT-IR spectra present the same profiles as the dried Mg–Al confirming the typical profiles of hydrotalcites. For the Co/Mg–Al(*T*) samples, small bands at 1365 and 1385 cm^{-1} can be related to the vibration of carbonates and nitrates into the interlayer, respectively. Nitrates derive from cobalt salt during the reconstruction phase and compensate positive charges of metal hydroxide layers. This result is in agreement with XRD study.

The regenerated structure of hydrotalcite is characterized by the broad band at around 3600 cm^{-1} and the band at 1645 cm^{-1} corresponding to OH groups.

For Co/Mg–Al(500), Co/Mg–Al(600) and Co/Mg–Al(700), a vibration band at 590 cm^{-1} is visible; its intensity is weaker for the support calcined at 700 °C. This band is an overlapping of vibrations attributed to Mg–O and Co–OH bonds [31]. The presence of Co–OH bond is quite probable since XRD results reveal the existence of CoOOH phase for these samples. Moreover, the absence of

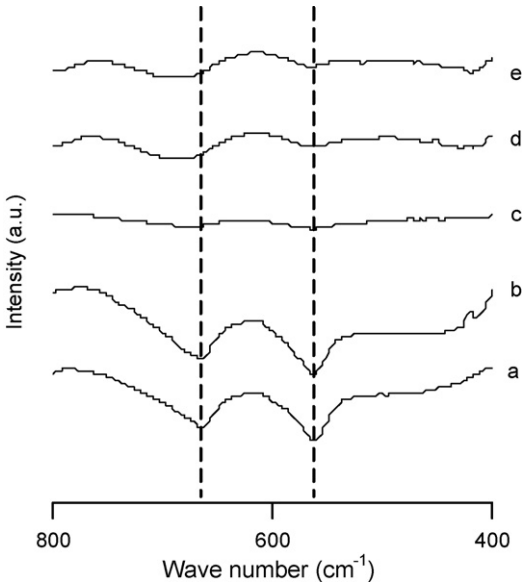

Fig. 4. IR spectra of Co/Mg–Al(*T*)500 (*T* = 500, 600, 700, 800 and 900 °C). (a) Co/Mg–Al(500)500; (b) Co/Mg–Al(600)500; (c) Co/Mg–Al(700)500; (d) Co/Mg–Al(800)500 and (e) Co/Mg–Al(900)500.

this band at 590 cm^{-1} for Co/Mg–Al(800) and Co/Mg–Al(900) is in agreement with XRD results.

Therefore, the IR study proves (i) the existence of the hydrotalcite reconstruction carried out in the presence of carbonates and nitrates (compensating anions) and (ii) the presence of "cobalt oxyhydroxide" phase for Co/Mg–Al(500), Co/Mg–Al(600) and Co/Mg–Al(700).

After that, IR of Co/Mg–Al(*T*) samples calcined at 500 °C is performed (Fig. 4). For all catalysts, two bands characterizing Co_3O_4 phase are detected. Their intensity is lower for samples calcined at higher temperatures, Co/Mg–Al(700)500, Co/Mg–Al(800)500 and Co/Mg–Al(900)500, than that of Co/Mg–Al(500)500 and Co/Mg–Al(600)500. Preudhomme et al. observed similar results with peaks at 672 and 590 cm^{-1} [32]. In our case, the latter band is shifted due to Al^{3+} and/or Mg^{2+} dissolution in Co_3O_4 [33].

The specific surface evolution of these solids after Co impregnation is quite interesting. A very significant decrease of the specific surface is observed for these samples compared with those obtained for the calcined supports (Table 1). Takehira et al. [34] explained that the formation of a dense layer of hydrotalcite type on the support surface is considered to be the main cause of this decrease. They also proved that low calcination temperature of Mg–Al (HT) solid promotes rapid reconstruction of hydrotalcite from the oxide phase "periclase" MgO. As a result, the regenerated hydrotalcite forms a dense film on the surface of "periclase" particles, blocking the penetration of cobalt ions into the pore structure of the Mg(Al)O. At higher calcination temperatures, the reconstruction of hydrotalcite is more difficult and takes place more slowly. In this case, the solution of cobalt nitrate can then diffuse into the pores of the oxide Mg(Al)O and spinel $MgAl_2O_4$. The calcination temperature of support plays a role in the regeneration of the hydrotalcite structure and, consequently, on the distribution and interaction between the cobalt active phase and the support. However, the decrease of the specific surface area is less important for Co/Mg–Al(800) and Co/Mg–Al(900). These results can be explained by a less important reconstruction of the calcined support at high temperature. Moreover, the high surface area for the solid impregnated on calcined HT at 800 and 900 °C suggests that (i) reconstitution of hydrotalcite takes place slowly and (ii) Co^{2+} nitrate solution penetrates into the pores of Mg–Al periclase oxide and $MgAl_2O_4$ spinel. These results are in accordance with the XRD observations (Fig. 2).

Table 2
EDX results over Co/Mg–Al(700) samples (at% calculated for Mg, Al and Co).

Co/Mg–Al(700) element	Point A		Point B		Point C	
	wt%	at%	wt%	at%	wt%	at%
Mg	26.33	65.65	18.73	65.70	2.98	12.28
Al	15.29	34.35	10.85	34.29	7.15	26.57
Co	–	–	–	–	35.93	61.15
Total	41.62	100	29.58	100	46.06	100

For a better understanding of the modification of solids related to the regeneration of the hydrotalcite structure, the surface morphology of the samples was studied by SEM–EDX analysis. Scanning Electron Microscopy (SEM) gives mainly morphological information, but when combined with Energy Dispersive detection of emitted X-ray photons, it offers the advantage of determining the chemical homogeneity of the catalysts at a mesoscopic scale. A distribution of the elements may be obtained. The hydrotalcite Mg–Al (HT) presents a platelet structure (Fig. 5a). After the calcination treatment, the morphology of the sample evolves, and the lamellar structure is significantly shrunken and broken (Fig. 5b). A significant change in the structure of solids occurs after impregnation of cobalt nitrate due to the reconstruction of the HT structure. Therefore, a disordered platelet structure forming irregular channel is observed (Fig. 5c).

The calcination then leads to an increase of the surface area observed by the porous aspect of the sample (Fig. 5d). The hydrotalcite surface reconstruction can be observed for the first time by the SEM image of the sample Co/Mg–Al(700) (Fig. 6). This picture (made in large magnification) clearly highlights three areas of particular morphologies. A composition analysis by SEM–EDX was performed at three points A, B and C representing the identified areas. The percentages of relative atomic mass of Mg, Al and Co elements measured at these points are reported in Table 2. The analysis results obtained for point A show that this area is rich in magnesium and aluminium and does not contain cobalt. The composition for the area A is like of the Mg–Al support. Moreover, the SEM image shows that no reconstruction has taken place in this area. The composition observed on point B is similar to that of point A. Thus, the particle analyzed is a grain of support that emerged as a result of the crushing of the sample. The EDX analysis of point C provides a high content of cobalt, and the Scanning Electron Microscopy image shows the hydrotalcite morphology. The formation of dense layer of cobalt enriched hydrotalcite on the surface of the Mg–Al support is then observed and explains the BET results.

The increase of specific area after calcination at 500 °C is then due to the mixed Co oxides surface structure and the porous aspect of the solid (Fig. 5c). XRD patterns of Co/Mg–Al(*T*)500 with *T* = 500, 600 and 700 samples are described in Ref. [25]. Diffraction peaks of MgO–periclase type and spinel structures Co_3O_4 and/or $CoAl_2O_4$ and/or Co_2AlO_4 are observed. The presence of the Co_3O_4 phase is probable for the impregnated solids, since cobalt oxyhydroxide phase is detected [25], and the calcination of this phase at 500 °C leads to the formation of Co_3O_4 spinel [35]. This result is in agreement with the IR study that reveals the presence of a band characteristic of Co–O bond of Co_3O_4 spinel phase (Fig. 3). However, the formation of the other spinel phases is possible since during the impregnation, cobalt is exchanged with magnesium in the brucite layers meaning that after calcination at 500 °C some cobalt aluminate oxides such as $Co_xAl_yO_4$ and $Co_xMg_yAl_zO_4$ can be formed. For samples with support treated at higher temperatures (Co/Mg–Al(800)500 and Co/Mg–Al(900)500), XRD patterns are pre-

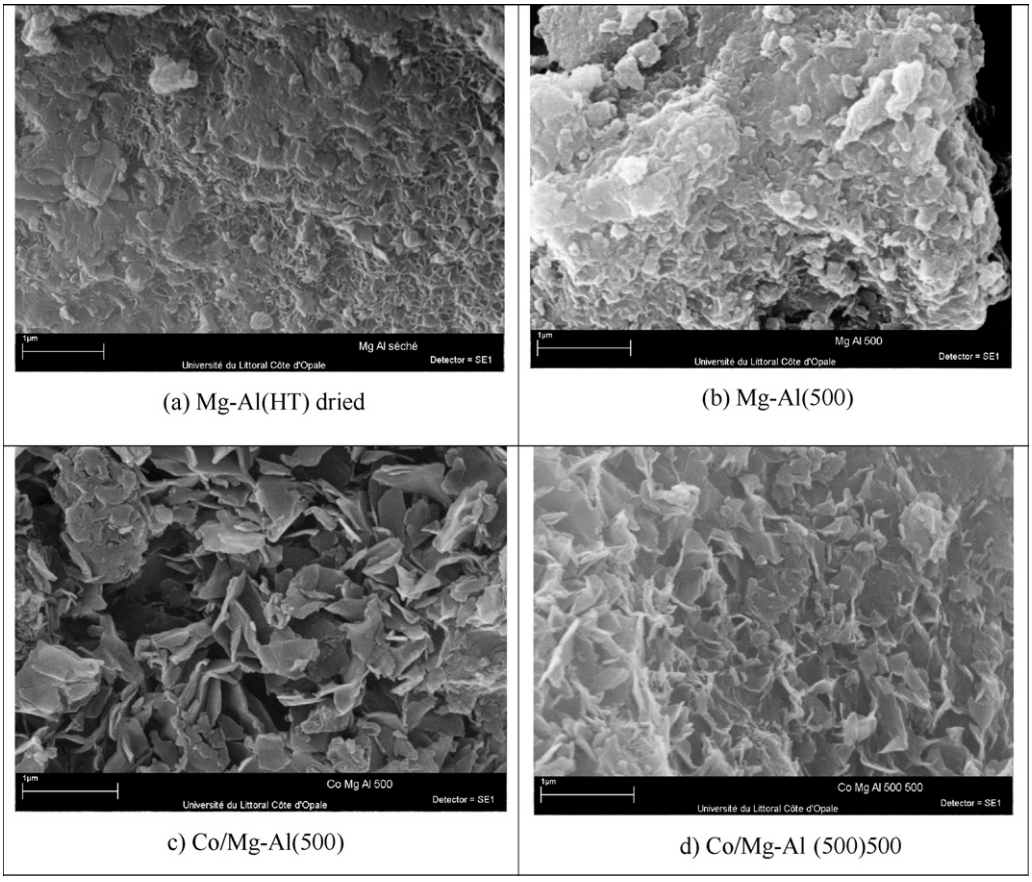

Fig. 5. SEM images of (a) Mg–Al(HT); (b) Mg–Al(500); (c) Co/Mg–Al(500) and (d) Co/Mg–Al(500)500.

sented in Fig. 7. $MgAl_2O_4$ phase is also detected with other phases described earlier.

H_2-TPR analysis of catalysts provides more information regarding the reducibility of oxide species. Knowing that Mg–Al support is not easily reducible, the consumed hydrogen can be assigned only to the reduction of cobalt species. Thus, many peaks are observed corresponding to different cobalt oxides in interaction with Mg–Al support. Co_3O_4 oxide type is reducible at low temperature (at around 330 °C) in two steps corresponding first to the reduction to CoO and then to metallic cobalt. However, it is not always easy to differentiate these steps. On the other hand, $CoAl_2O_4$ species, reduction occurs at higher temperature (around 700 °C). TPR profiles of Co/Mg–Al(*T*)500 catalysts seem to be influenced by the calcination of the support. TPR results for the samples Co/Mg–Al(500)500, Co/Mg–Al(600)500 and Co/Mg–Al(700)500 are described elsewhere [25]. Two groups of reduction peaks are observed: a first group corresponding to the reduction of Co_3O_4 to metallic cobalt and a second one at higher temperature corresponding to the reduction of cobalt species having an interaction with Mg and Al in the spinel matrix. As for Co/Mg–Al(800)500 and Co/Mg–Al(900)500, TPR profiles are displayed in Fig. 8. The same behaviour is observed except that the second peak is larger and shifted to higher temperature than that of catalysts with supports calcined at 500, 600 and 700 °C.

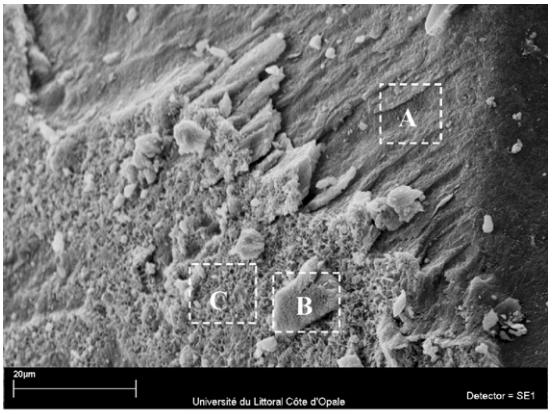

Fig. 6. SEM image of Mg–Al(700).

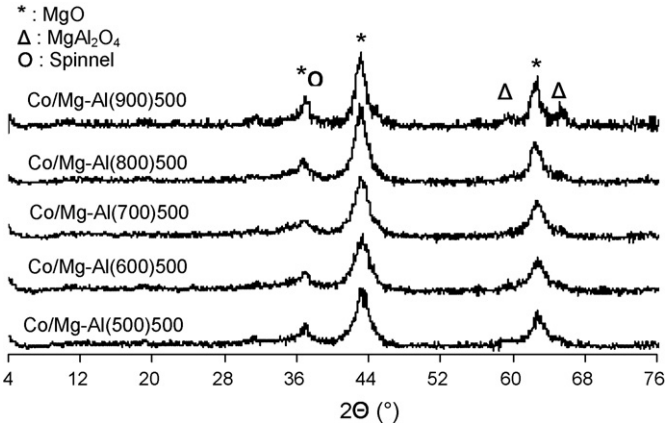

Fig. 7. XRD patterns of Co/Mg–Al(*T*)500 (*T* = 500, 600, 700, 800 and 900 °C) samples. Some patterns were already published in Ref. [24].

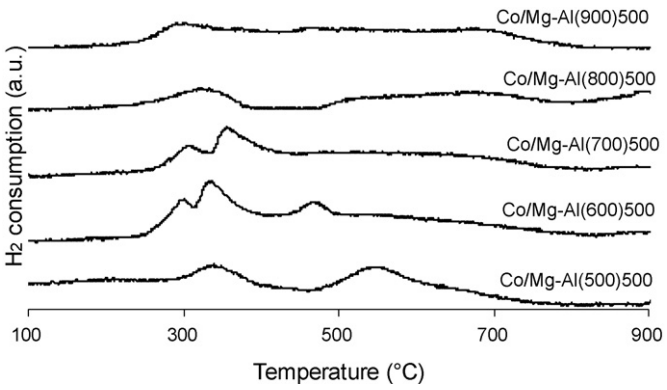

Fig. 8. TPR profiles of cobalt supported on Co/Mg–Al(*T*)500 (*T* = 500, 600, 700, 800, 900 °C). Some TPR profiles were already published in Ref. [24].

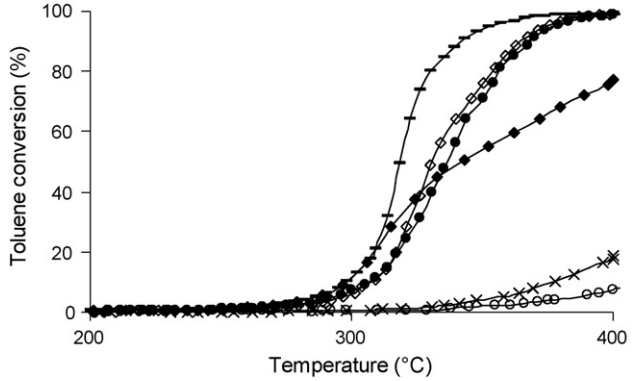

Fig. 9. Toluene conversion versus temperature for the samples: (×) Co/Mg–Al(500)500; (♦)Co/Mg–Al(600)500; (-) Co/Mg–Al(700)500, (■) Co/Mg–Al(800)500; (□) Co/Mg–Al(900)500; (Δ) Mg–Al(700). Some curves were already published in Ref. [24].

An increase of the hydrogen consumptions for peaks at lower temperature correlates with the existence of a higher amount of Co_3O_4 species than that of $CoAl_2O_4$.

Furthermore, the shift of Co_3O_4 reduction peaks to lower temperature is due to the existence of smaller particles well dispersed without interaction with the support. And the reduction of $CoAl_2O_4$ species occurring at higher temperature can be correlated to a spinel phase containing magnesium.

Therefore, reducibility of cobalt species depends on the nature of cobalt oxides and their interaction with the support. The step of the reconstruction is very important, and the degree of Mg and Co exchange influences the nature and the dispersion of the cobalt species on the support and the interaction with Mg and/or Al.

Fig. 9 details the catalytic behaviour of the samples towards toluene oxidation. According to T_{50} values, the catalytic performance of the used samples can be summarized in the following order:

Co/Mg–Al(700)500 > Co/Mg–Al(800)500 = Co/Mg–Al(900)500 > Co/Mg–Al(600)500 > Co/Mg–Al(500)500 > Mg–Al(700)

These results show that the catalysts are active for toluene oxidation. CO_2 and H_2O are the only products detected at 100% of conversion. The conversion of Mg–Al(700) compared to other catalysts presents a weaker activity with 10% of conversion at 400 °C. Thus, the use of cobalt has a beneficial effect on the activity. Moreover, the activity depends on calcination temperature of the support.

For example, a simple comparison between Co/Mg–Al(700)500 and Co/Mg–Al(500)500 samples reflects an interesting activity for the former (with a complete conversion at 350 °C), and a lesser catalytic activity, possibly the worse, for the latter.

Calcination at 500 °C leads to the formation of cobalt aluminate species knowing that these species are reduced at a higher temperature at about 550 °C [36]. Thus, the differences between the solids activities are related to the nature of cobalt species reduced at low temperature [15]. The catalytic behaviour can be then related to the reducibility of cobalt oxides species: the higher is the reducibility the higher is the catalytic activity. The TPR profiles and the H_2 consumption of Co/Mg–Al(800)500 and Co/Mg–Al(900)500 samples are similar and reflect the same catalytic activity. Besides, the samples Co/Mg–Al(600)500 and Co/Mg–Al(700)500 present similar hydrogen consumptions and catalytic behaviours at around 300 °C. However, a decrease in activity is noticed for temperatures higher than 300 °C for Co/Mg–Al(600)500. This result could be explained by a possible instability of the solid related to the presence of water during the catalytic test. The calcination at 600 °C is too low to obtain stable MgAlO, the presence of "metahydrotalcite P periclase amorphous" phase (XRD) confirming this result.

4. Conclusion

The study has revealed that, even though calcined at high temperature, a Mg–Al mixed oxides support was partly rebuilt as a layered double hydroxide during the cobalt impregnation. That structural modification of the support is accompanied by a significant decrease in the specific area. Moreover, it has been shown that the calcination temperature of the support influences the reconstruction of the layered structure and, consequently, the interaction between cobalt species and the support. The hydrotalcite regeneration was shown by IR and SEM–EDX analysis. The latter has identified areas of reconstruction rich in cobalt. The calcination at 500 °C of Co/Mg–Al(700) leads to an interesting Co catalyst supported on calcined hydrotalcite with a high specific area and a high potential for toluene deep oxidation. Thus, the reconstruction of the support can generate high quantity of active surface cobalt species. And their activity can be correlated to their high reducibility at low temperature.

Acknowledgements

This work is supported by the "Région Nord Pas de Calais", Interreg IV "Redugaz" project and the European Community (European Regional Development Fund). Dr. Lucie Courcot is also acknowledged for SEM–EDX analysis.

References

[1] K. Everaert, J. Baeyens, J. Hazard. Mater. B 109 (2004) 113.
[2] A. O'Malley, B.K. Hodnett, Catal. Today 54 (1999) 31.
[3] G. Centi, J. Mol. Catal. A 173 (2001) 287.
[4] J.-M. Giraudon, A. Elhachimi, F. Wyrwalski, S. Siffert, A. Aboukaïs, J.-F. Lamonier, G. Leclercq, Appl. Catal. B 75 (2007) 157.
[5] C. Gennequin, M. Lamallem, R. Cousin, S. Siffert, F. Aïssi, A. Aboukaïs, Catal. Today 122 (2007) 301.
[6] M. Hosseini, S. Siffert, H.L. Tidahy, R. Cousin, J.-F. Lamonier, A. Aboukais, A. Vantomme, M. Roussel, B.-L. Su, Catal. Today 122 (2007) 391.
[7] S.C. Kim, J. Hazard. Mater. B 91 (2002) 285.
[8] C. Lahousse, A. Bernier, P. Grange, B. Delmon, P. Papaefhimiou, T. Loannides, X. Verykios, J. Catal. 178 (1998) 214.
[9] C. Gennequin, S. Siffert, R. Cousin, A. Aboukais, Top. Catal. 52 (2009) 482.
[10] J. Tsou, P. Magnoux, M. Guisnet, J.J.M. Orfao, J.L. Figueiredo, Appl. Catal. B: Environ. 51 (2004) 129.
[11] H.L. Tidahy, S. Siffert, F. Wyrwalski, J.-F. Lamonier, A. Aboukais, Catal. Today 119 (2007) 317.
[12] F. Bertinchamps, C. Grégoire, E.M. Gaigneaux, Appl. Catal. B 6 (2006) 1.
[13] M. Baldi, E. Finocchio, F. Millela, G. Busca, Appl. Catal. B 16 (1998) 43.
[14] F.G. Duran, B.P. Barbero, L.E. Cadus, C. Rojas, M.A. Centeno, J.A. Odriozola, Appl. Catal. B 92 (2009) 194.
[15] F. Wyrwalski, J.-F. Lamonier, S. Siffert, L. Gengembre, A. Aboukaïs, Catal. Today 119 (2007) 332.

[16] P.-O. Larsson, H. Berggren, A. Andersson, O. Augustsson, Catal. Today 35 (1997) 137.
[17] K. Jiratova, P. Cuba, F. Kovanda, L. Hilaire, V. Pitchon, Catal. Today 76 (2002) 43.
[18] I. Dobrosz, K. Jiratova, V. Pitchon, J.M. Rynkowski, J. Mol. Catal. A 234 (2005) 187.
[19] D. Tichit, C. Gérardin, R. Durand, B. Coq, Top. Catal. 39 (2006) 89.
[20] D.P. Debecker, E.M. Gaigneaux, G. Busca, Chem. Eur. J. 15 (2009) 3920.
[21] F. Cavani, F. Trifiro, A. Vaccari, Catal. Today 11 (1991) 173.
[22] J. Sanchez Valente, F. Figueras, M. Gravelle, P. Kumbhar, J. Lopez, J.-P. Besse, J. Catal. 189 (2000) 370.
[23] A. Alejandre, F. Medina, X. Rodriguez, P. Salagre, Y. Cesteros, J.E. Sueiras, Appl. Catal. B 30 (2001) 195.
[24] A. Vaccari, Catal. Today 41 (1998) 53.
[25] C. Gennequin, R. Cousin, J.-F. Lamonier, S. Siffert, A. Aboukais, Catal. Commun. 9 (2008) 1639.
[26] F. Millange, R.I. Walton, D. O'Hare, J. Mater. Chem. 10 (2000) 1713.
[27] T. Staminirova, I. Vergilov, G. Kirov, J. Mater. Sci. 34 (1999) 4153.
[28] F. Kovanda, K. Jiratova, J. Rymes, D. Kolousek, Appl. Clay Sci. 18 (2001) 71.
[29] W. Yang, Y. Kim, P.K.T. Liu, M. Sahimi, T. Tsotsis, Chem. Eng. 57 (2002) 2945.
[30] T. Staminirova, G. Kirov, Appl. Clay Sci. 22 (2003) 295.
[31] J.T. Kloprogge, R.L. Frost, Appl. Catal. A: Gen. 184 (1999) 61.
[32] J. Preudhomme, P. Tarte, Spectrochim. Acta 27A (1971) 1817.
[33] L. Obalova, K. Jiratova, F. Kovanda, K. Pacultova, Z. Lacny, Z. Mikulova, Appl. Catal. B: Environ. 60 (2005) 289.
[34] K. Takehira, T. Shishido, D. Shoro, K. Murakami, M. Honda, T. Kawabata, K. Takaki, Appl. Catal. A 279 (2005) 41.
[35] Z.P. Xu, H.C. Zeng, J. Mater. Chem. 8 (11) (1998) 2499.
[36] P. Arnoldy, J.A. Moulijn, J. Catal. 93 (1985) 38.
[37] Y.-J. Lin, D.-Q. Li, D.G. Evans, X. Duan, Polym. Degrad. Stab. 88 (2005) 296.